Viscous/Inviscid Analysis of Transonic Shock-Induced Separation Including Normal Pressure Gradients

D. E. Edwards* and J. E Carter†
United Technologies Research Center, East Hartford, Connecticut
and
M. M. Hafez‡
Computer Dynamics, Inc., Hampton, Virginia

An analysis based on an interacting boundary-layer theory is presented for the prediction of transonic shock-wave/boundary-layer interaction with emphasis on turbulent separated flow. In this analysis, finite difference techniques are used to iteratively solve the viscous layer equations, expressed in a defect form, coupled to a stream function representation of the inviscid flow. Normal pressure gradients and imbedded shock effects are included in this analysis. Favorable comparisons obtained with the separated flow data of Kooi demonstrate that, for transonic shock-induced separation, the effect of displacement thickness interaction dominates over that produced by imbedded shock effects and normal pressure gradients. Calculations made with a modified algebraic turbulence model demonstrate that, for separated flow cases, the computed results are more sensitive to the turbulence model than to whether or not normal pressure gradients are included.

Introduction

THE prediction of the flowfield in transonic shock-wave/boundary-layer interaction is an aerodynamic problem of immense practical importance in both external aerodynamics and turbomachinery applications since this flow phenomenon has a large influence on the overall aerodynamic forces and often determines the upper limit in performance of each aerodynamic component. The intersection of a shock wave with a turbulent boundary layer in transonic flow results in a complex flow pattern, as shown in Fig. 1 for separated flow. Flow separation generally results in a bifurcation of the shock wave into a front and rear leg near the wall, with a vortex sheet emanating from the triple point. A separation bubble of slow recirculating flow occurs at the foot of the shock wave in the lower portion of the viscous layer. The short streamwise length scale of the interaction region results in a rapid turning of the flow that is generally thought to induce large normal pressure gradients in the viscous layer. The overall objective of the present paper is to present a reliable and accurate method for the prediction of the detailed properties of the flow occurring when a transonic normal shock wave, of sufficient strength to cause flow separation, impinges on a turbulent boundary layer. Only the flow in the immediate vicinity of the shock-wave/boundary-layer interaction has been considered, since the focus of the present work was to use the analysis developed herein to give a better understanding of the relative importance of imbedded shock effects and normal pressure gradients in transonic shock-induced separation.

Numerous attempts have been made in recent years to develop an improved theoretical understanding of transonic shock-wave/boundary-layer interaction. These approaches range from the asymptotic analyses by Melnik and Grossman,[1] Adamson and Feo,[2] and Messiter[3] to a more general treatment through the numerical solution of the Reynolds-averaged Navier-Stokes equations, such as the work of Viegas and Horstman[4] and Shea.[5] An excellent review of recent work on transonic shock-wave/boundary-layer interaction is presented by Adamson and Messiter.[6] Despite the advances made in this previous work, there still exist significant limitations that must be overcome in order to develop a reliable, accurate prediction method for transonic shock-induced separation. In particular, the asymptotic methods are currently limited to weak shock waves for which the flow remains attached; alternately, accurate numerical solutions for the Navier-Stokes equations are difficult due to the requirement that the grid must be carefully chosen to capture the flow phenomenon occurring at different length scales in the interaction problem.

A different approach has been taken in the present paper that is based on the concepts of interacting boundary-layer theory (IBLT). This approach assumes that, for high Reynolds numbers, the flow can be divided into viscous and inviscid regions even if flow separation is present. In recent years it has been successfully demonstrated that IBLT can be used to provide an accurate description for subsonic strongly interacting flows in which the separation is induced by a continuous adverse pressure gradient. For discontinuous pressure gradients, that is, shock-induced separated flows, a generalized IBLT model based on the defect formulation developed by LeBalleur,[7] and subsequently utilized by East[8] and Lock and Firmin,[9] has been adopted for the present study. In defect formulation the governing equations in the viscous layer are expressed as the difference (or defect) between the viscous and inviscid flow equations. Although this model is not based on a rational asymptotic expansion of the Navier-Stokes equations, the defect formulation permits the generalization of IBLT to include the imbedded shocks and normal pressure gradients in the viscous region that are generally thought to be significant in transonic shock-induced separated flow.

The present paper, which is a condensed version of Ref. 10, presents a generalized viscous-inviscid interaction flow model that consists principally of a differential treatment of the defect formulation laid out by LeBalleur,[7] utilizing a generalization of the inverse boundary-layer method of

Presented as Paper 85-0371 at the AIAA 23rd Aerospace Sciences Meeting, Reno, NV, Jan. 14-17, 1985; received Feb. 1, 1985; revision received Sept. 27, 1985.

*Research Engineer. Member AIAA.
†Manager, Computational Fluid Dynamics. Member AIAA.
‡Presently, Professor, Department of Mechanical Engineering, University of California. Member AIAA.

Carter[11] coupled to the inviscid stream function method of Hafez and Lovell.[12] The experimental data of Kooi[13,14] is used to evaluate this approach. Numerous conclusions are drawn from the present study; the principal one is that displacement thickness coupling is the dominant effect that must be included in the prediction of separated transonic shock-wave/boundary-layer interaction.

Analysis

Formulations of the viscous and inviscid flow regions are presented in this section followed by a discussion of the viscous-inviscid interaction procedure that is used to couple the two flow analyses. In addition, a brief discussion of an improved algebraic turbulence model developed in this investigation is presented.

Viscous Formulation

It is assumed that the Reynolds number is sufficiently large for the flowfield to be represented by interacting boundary-layer theory, whereby the entire flowfield is divided into a viscous region near the surface and an inviscid region outside of the viscous layer. At a sufficiently large distance from the surface, the viscous solution is required to merge smoothly into that for the inviscid flow as shown in Fig. 2 for the u component of velocity. Therefore, it is convenient to write the viscous layer equations as the difference between the real viscous flow (RVF) and the equivalent inviscid flow (EIF), where the latter results when the inviscid flow is solved in the interior of the viscous region. LeBalleur[7] was the first to write the viscous equations in this defect form; Lock and Firmin[9] have further explored this and introduced the concepts of RVF and EIF mentioned above.

The defect form of the nondimensional viscous-layer equations used in the present study is written as follows in terms of the x,y Cartesian coordinates and the corresponding components, u and v, in which the i subscript is used to denote the variables in the EIF:

$$\frac{\partial(\psi-\psi_i)}{\partial y}=\rho u-\rho_i u_i \tag{1}$$

$$\rho u\frac{\partial u}{\partial x}-\rho_i u_i\frac{\partial u_i}{\partial x}-\frac{\partial\psi}{\partial x}\frac{\partial u}{\partial y}+\frac{\partial\psi_i}{\partial x}\frac{\partial u_i}{\partial y}$$
$$=-\frac{\partial\hat{p}}{\partial x}+\frac{1}{Re_\infty}\left[\frac{\partial}{\partial y}(\mu+\epsilon)\frac{\partial u}{\partial y}\right] \tag{2}$$

where $\hat{p}=p-p_i$. For this study, as will be discussed later, $\hat{p}$ is assumed to equal zero. It has been found convenient to replace the v component of velocity in the viscous-layer equations with the stream function, using the relation $\partial\psi/\partial x=-\rho v$ with the continuity equation now replaced with Eq. (1). An eddy viscosity representation given by $(\epsilon/Re_\infty)\partial u/\partial y=-\rho\overline{u'v'}$ has been used in Eq. (2) to represent the Reynolds stress. The variables in Eqs. (1) and (2) are expressed in nondimensional form with lengths scaled by the upstream boundary-layer thickness δ_0^*, velocities by the freestream value u_∞^*, pressure by twice the freestream dynamic pressure $\rho_\infty^* u_\infty^{*2}$, density by ρ_∞^*, and viscosity coefficients by μ_∞^*. An asterisk is used to denote dimensional quantities. The Reynolds number appearing in Eq. (2) is given by $Re_\infty=\rho_\infty^* u_\infty^* \delta_0^*/\mu_\infty^*$. The viscous formulation is completed with the Sutherland relation for the molecular viscosity, the state equation, and the assumption of constant total enthalpy since only adiabatic flows have been treated.

It is observed that the EIF in Eqs. (1) and (2) has been expressed in terms of the Euler equations instead of the stream function equation used to represent the inviscid flow, as will be described later in this section. This step is taken to ensure

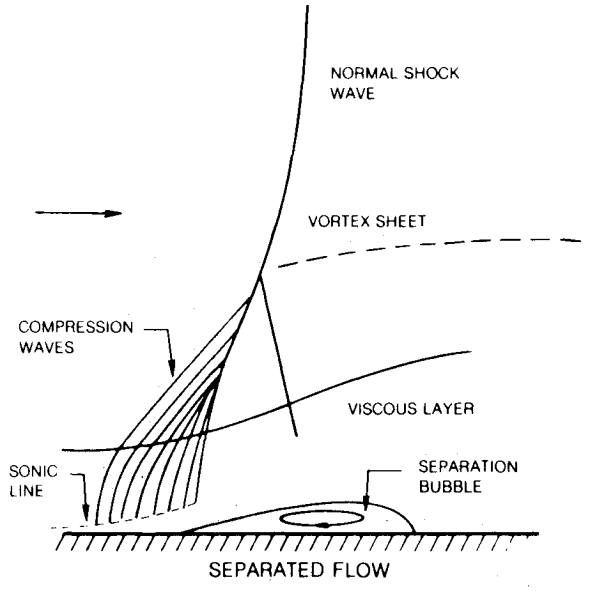

Fig. 1 Normal shock wave impinging on a turbulent boundary layer.

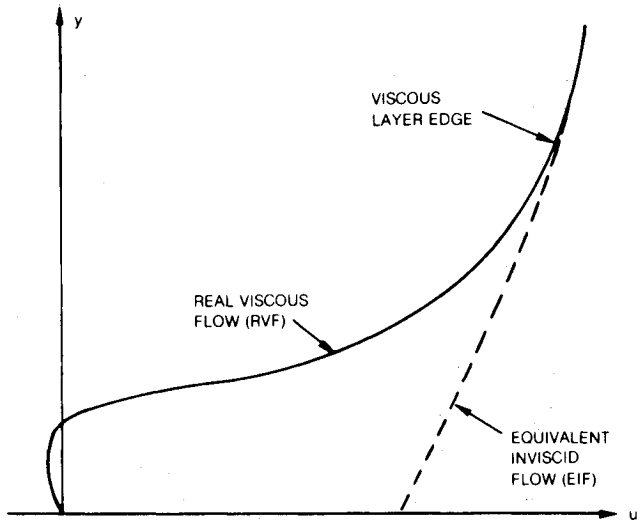

Fig. 2 Viscous-inviscid matching of velocity profile.

that, as the edge of the viscous layer is approached, the imposition of the boundary conditions

$$u\to u_i,\quad \psi\to\psi_i \tag{3}$$

results in a smooth merging of the viscous and inviscid solutions as shown in Fig. 2 for the u component of velocity. At the surface, $y=0$, the usual viscous boundary conditions

$$u=0,\quad \psi=0 \tag{4}$$

are imposed.

Transformed Viscous Formulation

Based on previous work in the analysis of separated viscous flows,[11] the finite difference solutions of the governing equations are facilitated by the use of a modified form of the Levy-Lees transformation, which is given by

$$\xi=\int_0^x \rho_{ir}u_{ir}\mu_{ir}dx\quad \hat{\eta}=\frac{y}{\delta^*}h(x)=\eta h(x) \tag{5}$$

where the *ir* subscripted quantities denote the inviscid solution at a reference surface such as the wall or displacement body, and the function $h(x)$ is used to control the laternal extent of the computational region of the viscous analysis. In this investigation, $h(x)$ was set to δ^*/δ, where δ is the boundary-layer thickness.

In the present analysis, the inviscid flow is permitted to vary over the viscous-layer thickness due to the strong viscous-inviscid interaction that occurs when a transonic shock wave impinges on a turbulent boundary layer. Therefore, it is necessary to account for this inviscid variation by generalizing the displacement thickness definition to

$$\int_{\delta^*}^{\delta} \rho_i u_i \mathrm{d}y = \int_0^{\delta} \rho u \mathrm{d}y \tag{6}$$

which states that the mass flow in the EIF is equal to that in the RVF. In the present investigation, it has been found convenient to use an alternative displacement thickness definition given by

$$\delta^* = \frac{1}{\rho_{ir} u_{ir}} \int_0^{\delta} (\rho_i u_i - \rho u) \mathrm{d}y \tag{7}$$

Lock and Firmin[9] have explored the difference in these two definitions of δ^* and have concluded that they differ less from each other than they do from the classical definition obtained by setting $\rho_i u_i = \rho_e u_e$ in Eqs. (6) and (7), which leads to

$$\delta^* = \int_0^{\delta} \left(1 - \frac{\rho u}{\rho_e u_e}\right) \mathrm{d}y \tag{8}$$

where $\rho_e u_e$ is constant across the boundary layer.

In the viscous layer, it is convenient to use a perturbation stream function $\tilde{f}$ to represent the difference between the viscous and inviscid stream functions written as

$$\psi - \psi_i = m(1 - \tilde{f}) \tag{9}$$

where $m = \rho_{ir} u_{ir} \delta^*$ is the perturbation mass flow. As $y \to \infty$, $\tilde{f} \to 1$, so that the viscous stream function merges smoothly with that of the inviscid solution. At the surface $y = 0$, the usual boundary condition $\psi = 0$ is imposed by setting $\tilde{f} = 0$, since at the wall the displacement thickness induced inviscid stream function is set to

$$\psi_i(x,0) = -m \tag{10}$$

A detailed derivation of this inviscid surface boundary condition is presented in Ref. 10.

In first-order theory, where the inviscid flow velocity is invariant on the scale of boundary layer, the inviscid stream function varies linearly in the viscous region. Hence, a second perturbation stream function ψ_Δ is introduced that denotes the deviation of the inviscid stream function from its first-order linear variation. This function is given by

$$\psi_\Delta = \psi_i - m(\eta - 1) \tag{11}$$

which when combined with Eq. (9) yields the following form for the viscous stream function:

$$\psi = m(\eta - \tilde{f}) + \psi_\Delta \tag{12}$$

The defect form of the viscous-layer equations given in Eqs. (1) and (2) is transformed with the independent variables given in Eq. (5) and the dependent variables, other than the stream function, scaled as follows by the inviscid solution at the reference surface:

$$F = \frac{u}{u_{ir}}, \quad F_i = \frac{u_i}{u_{ir}}, \quad \bar{\rho} = \frac{\rho}{\rho_{ir}}, \quad \overline{\rho_i} = \frac{\rho_i}{\rho_{ir}}, \quad \bar{\mu} = \frac{\mu}{\mu_{ir}}, \quad \bar{\epsilon} = \frac{\epsilon}{\mu_{ir}} \tag{13}$$

The transformed equations become

$$\frac{\partial \tilde{f}}{\partial \hat{\eta}} = \frac{1}{h}(1 - \bar{\rho}F) + \frac{1}{m}\frac{\partial \psi_\Delta}{\partial \hat{\eta}} \tag{14}$$

$$\begin{aligned} m^2 \bar{\rho} F \frac{\partial F}{\partial \xi} - mh \frac{\partial}{\partial \xi}\left[m\left(\frac{\hat{\eta}}{h} - \tilde{f}\right) + \psi_\Delta\right]\frac{\partial F}{\partial \hat{\eta}} \\ = m^2 \overline{\rho_i} F_i \frac{\partial F_i}{\partial \xi} - mh \frac{\partial}{\partial \xi}\left[m\left(\frac{\hat{\eta}}{h} - 1\right) + \psi_\Delta\right]\frac{\partial F_i}{\partial \hat{\eta}} \\ + m^2 \beta(\overline{\rho_i} F_i^2 - \bar{\rho} F^2) + \frac{h^2}{Re_\infty}\frac{\partial}{\partial \hat{\eta}}\left[(\bar{\mu} + \bar{\epsilon})\frac{\partial F}{\partial \hat{\eta}}\right] \end{aligned} \tag{15}$$

The boundary conditions imposed on the viscous formulation are given by

$$\hat{\eta} = 0, \quad F = \tilde{f} = 0 \tag{16}$$

$$\hat{\eta} \to \infty, \quad F \to F_i, \quad \tilde{f} \to 1 \tag{17}$$

The imposition of an outer boundary condition on the stream function permits these equations to be solved in the inverse form, that is, the unknown pressure gradient parameter $\beta = (1/u_{ir})/(\mathrm{d}u_{ir}/\mathrm{d}\xi)$ is deduced along with the viscous solution for a prescribed distribution of the perturbation mass flow m. This approach allows the present generalized viscous formulation to be incorporated into the interaction iteration procedure that has been successfully used in numerous studies[15] on first-order viscous-inviscid interaction. It is observed that the present analysis is easily reverted back to a first-order formulation in which the inviscid flow quantities are invariant across the boundary layer by setting $F_i = \bar{\rho}_i = \bar{T}_i = 1$, and $\psi_\Delta = 0$. In this case $u_i = u_e$, $\rho_i = \rho_e$, $p_i = p_e$ where the edge quantities, denoted by the e subscript, are constant at each x station along the surface.

Equivalent Inviscid Flow

The inviscid flow solution in the interior of the viscous layer, which is referred to as the equivalent inviscid flow (EIF), is required for two purposes in the present viscous-layer formulation. First, it is needed since the viscous equations have been written as the difference (defect form) between the EIF and the real viscous flow (RVF); and second, in the present calculations, the viscous streamwise pressure gradient has been approximated as the inviscid streamwise pressure gradient ($\hat{p} = 0$) for $y > \delta^*$. Below $y = \delta^*$, it is assumed that the streamwise pressure gradient is now independent of y and equal to that of the EIF at the displacement surface, which is a reasonable approximation for $y < \delta^*$ since it is known that the normal pressure gradient in the RVF is zero at the flat wall. This treatment of normal pressure gradients assumes that the pressure variation across the outer part of the viscous layer is that of the inviscid flow induced by the rapidly curving displacement surface. It is recognized that this treatment is approximate but, as pointed out by LeBalleur,[7] it is more complete than the Prandtl assumption of constant pressure across the boundary layer. If warranted, a more general defect formulation, which includes the normal momentum equation, is available as originally shown by LeBalleur and derived for the present approach in Ref. 10.

In order to accommodate this treatment of the pressure gradient, the inviscid reference surface, about which the

viscous formulation is normalized, has been chosen as the displacement surface at $\eta = 1$. Hence, the *ir* subscripted quantities have been taken as the inviscid solution at $y = \delta^*$. In the global viscous-inviscid interaction procedure, just before the viscous solution is updated, the required input from the EIF is computed. Using the current value of δ^*, linear interpolation in the y direction is performed at each x station to determine the inviscid u component of velocity and the density at $y = \delta^*$. Denoting these values as $u_{ir} = u_\delta^*$ and $\rho_{ir} = \rho_\delta^*$, respectively, we now compute the $\hat{\eta}$ distribution of

$$F_i = u_i/u_\delta^*, \quad \overline{\rho_i} = \rho_i/\rho_\delta^* \tag{18}$$

and the perturbation inviscid stream function ψ_Δ from

$$\psi_\Delta = \frac{m}{h}\int_0^{\hat{\eta}} (\overline{\rho_i} F_i - 1)\, d\hat{\eta} \tag{19}$$

using the trapezoidal rule of integration. Below the displacement thickness $F_i = \bar{\rho}_i = 1$ and thus $\psi_\Delta = 0$ in this region, so that the y dependence of the inviscid streamwise pressure gradient is eliminated.

The viscous-layer equations with the imposed EIF are solved with an implicit finite difference that is first-order accurate in the ξ coordinate and second-order accurate in the $\hat{\eta}$ coordinate. The finite difference representation of the EIF terms is treated identically to the corresponding viscous flow convection terms, thereby insuring that these terms are numerically in balance as the edge of the viscous layer is approached. Other than the inclusion of the EIF terms, the numerical treatment is identical to that used previously in the first-order viscous analysis.[11]

Inviscid Formulation

The inviscid solution used in the present study was obtained from the numerical solution of the second-order stream function equation

$$\frac{\partial}{\partial x}\left(\frac{1}{\rho_i}\frac{\partial \psi_i}{\partial x}\right) + \frac{\partial}{\partial y}\left(\frac{1}{\rho_i}\frac{\partial \psi_i}{\partial y}\right) = -\omega \tag{20}$$

which is obtained from combining the definitions of vorticity and stream function. The numerical method used to solve Eq. (20) is that developed by Hafez and Lovell[12] for transonic flow. Prior to their work, difficulties had been encountered in the use of the stream function approach in the transonic speed range, since the density is a double-valued function of the mass flux (there is a subsonic and supersonic branch). Hafez and Lovell presented a method that overcomes this difficulty, thereby allowing solutions to the stream function equation to be obtained for transonic flows. This approach has a major advantage over that based on the potential flow approximation since it is equivalent to a solution of the Euler equations, provided the entropy and vorticity produced by a curved shock or an upstream nonuniformity are taken into acount. In the present calculations, the vorticity is set to zero since the upstream flow is assumed uniform and the shock is assumed to be straight. However, the usefulness of the Hafez and Lovell approach for rotational inviscid flows is demonstrated in Ref. 10, in which predicted solutions are shown to be in good agreement with the asymptotic theory results of Melnik and Grossman[1] for a weak shock wave impinging on a turbulent boundary layer.

The computational region for the analysis of a normal shock wave impinging on a flat-plate boundary layer is shown in Fig. 3. At the upstream boundary AB, the incom-

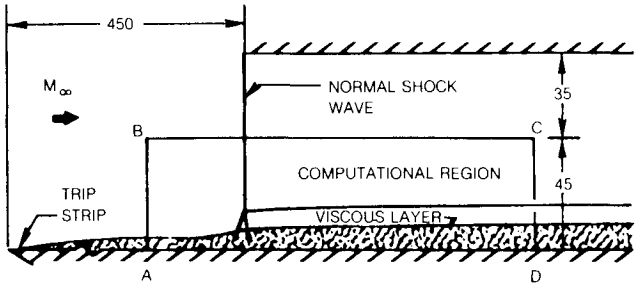

Fig. 3 Kooi experimental configuration and present computational region (ABCD) (all dimensions in millimeters).

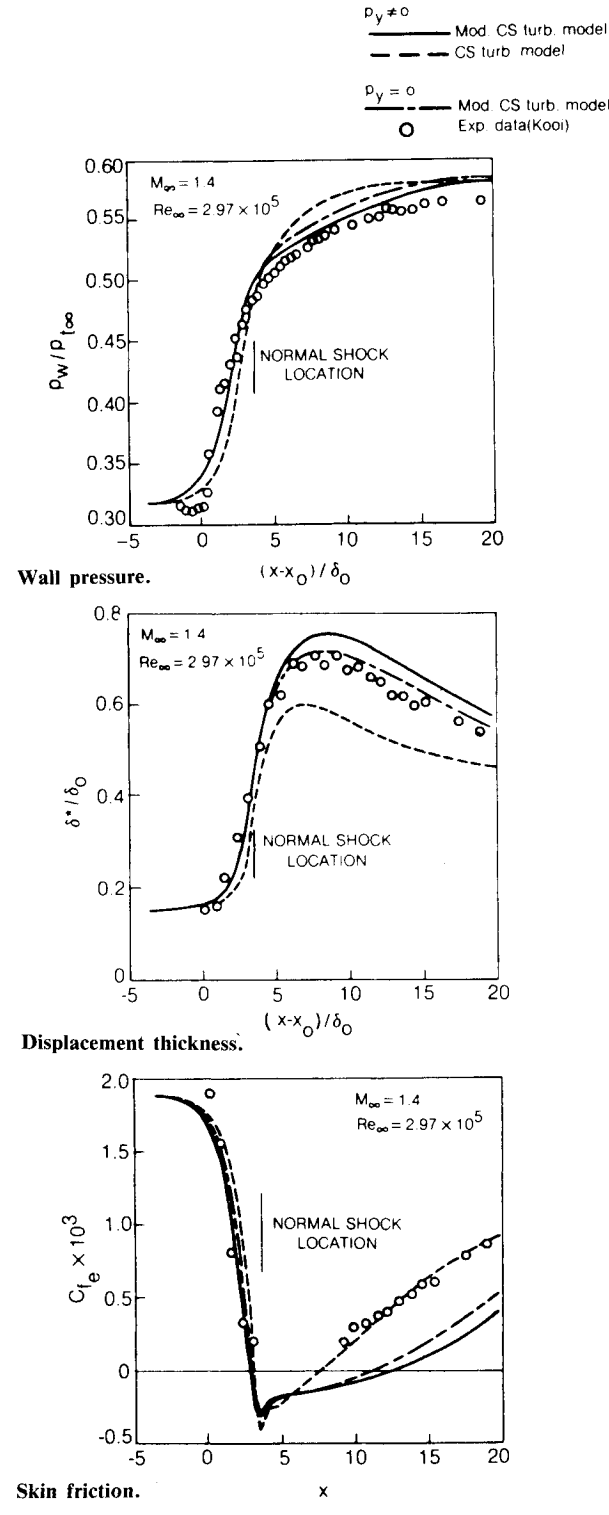

Fig. 4 Comparison of results from IBLT with experimental data for transonic normal shock-wave/boundary-layer interaction.

ing flow is assumed to be uniform, $u_i = 1$. At the downstream boundary CD, $\psi_{i_{xx}} = 0$; calculations were also made with $\psi_{i_x} = 0$ at this boundary with only small changes in the results. As previously mentioned, at the wall AD, the viscous induced displacement thickness condition, $\psi_i(x,0) = -m$, is imposed. For the calculations made to compare the present method with the experimental data of Kooi,[13,14] it was found necessary (as shown in Ref. 10) to impose conditions along the outer boundary BC to represent the boundary-layer blockage effects existing when a shock-wave/boundary-layer interaction occurs in a tunnel. The conditions imposed are

$$\frac{\partial \psi_i}{\partial y} = \rho_i u_i \tag{21}$$

where the prescribed distribution of $\rho_i u_i$ along BC was deduced from the experimentally measured static pressure and the assumption that the total pressure along BC is held constant.

Viscous-Inviscid Interaction

The iteration procedure used in the present study to couple the transonic stream function analysis to the viscous formulation is a generalization of a procedure[11] that has been successfully applied in numerous computations of first-order viscous-inviscid interactions. In this method, the displacement thickness parameter m is simultaneously specified for a direct (shape-prescribed) solution of the inviscid equations and for an inverse solution of the viscous-layer equations. This parameter is then updated based on the following update formula:

$$m^{\nu+1} = m^{\nu}\left[1 + \bar{\omega}\left(\frac{u_{\delta_v^*}}{u_{\delta_i^*}} - 1\right)\right] \tag{22}$$

where $\bar{\omega}$ is the relaxation factor.

In Eq. (22), $u_{\delta_v^*}$ and $u_{\delta_i^*}$ denote the viscous and inviscid predictions, respectively, of the inviscid velocity along the displacement surface. In the computed results, to be presented in the next section, the quantity $u_{\delta_i^*}$ has been approximated as the inviscid velocity at the wall u_w. This approximation was made to eliminate minor oscillations that resulted when $u_{\delta_i^*}$ was used in the update expression. These oscillations are probably due to the interpolation required in the inviscid calculation to find $u_{\delta_i^*}$, since the grid is aligned to the wall and not to the displacement surface. This approximation has a relatively small effect on the results, since the inviscid flow changes only slightly between the wall and the displacement body.

Modified Algebraic Turbulence Model

It is well known that use of the Cebeci-Smith (CS) algebraic turbulence model[16] generally results in the overprediction of the pressure and an underprediction of the displacement thickness in the analysis of separated turbulent flow. In the past, it has been found that some improvement in the predicted results could be obtained by a reduction in the local values of the eddy viscosity coefficient predicted by this model. One example of this type of modification is the Shang-Hankey[17] relaxation model, which has been used by a number of investigators for the computation of separated turbulent flow. In this model, both the inner and outer layer eddy viscosity levels are constrained to depart by only a specified amount from an upstream equilibrium boundary-layer level. More recently, a simple numerical experiment by Carter[18] demonstrated that a reduction in the outer region length scale, which Clauser[19] deduced as the incompressible displacement thickness for mild pressure gradient flow, resulted in similar improvements of the separated flow predictions as demonstrated by others with the Shang-Hankey model. In the study conducted by Edwards,[20] the incompressible turbulent separated flow data of Simpson et al.[21] was examined to determine if the length scale used in the eddy viscosity of the outer viscous region could be inferred from their detailed measurements for the streamwise velocity profiles and the Reynolds stress distributions. It was found that if the outer eddy viscosity coefficient was based on the incompressible momentum thickness instead of the incompressible displacement thickness, a substantial improvement was found in the correlation of the maximum Reynolds shear stress with the local gradient of the mean velocity profile for incompressible separated flow. With this modification, the outer region eddy viscosity coefficient is expressed as

$$\epsilon/\mu = 0.0168\ H_F(\rho/\mu)u_e\theta_{\text{inc}} \tag{23}$$

where the quantity H_F is the flat-plate incompressible shape factor $\delta^*_{\text{inc}}/\theta_{\text{inc}}$, which is equal to 9/7, and the quantity θ_{inc} is the incompressible momentum thickness. For flat-plate flows, this model is identical to Clauser's model. As will be seen in the next section, this modified Cebeci-Smith (CS) turbulence model has improved the present predictions for transonic shock-wave/boundary-layer interaction. Although a physical explanation of this improvement is lacking, the use of θ_{inc} instead of δ^*_{inc} as the length scale in the outer layer tends to reduce the streamwise growth of ϵ in a similar manner as the numerical experiment in Ref. 18 and in the Shang-Hankey model. It is interesting to note that a detailed examination of Clauser's original work,[19] in which the classical outer layer eddy viscosity model was presented, shows that the length scale could be θ_{inc} instead of δ^*_{inc} with a suitable adjustment in the constant of proportionality.

Results and Discussion

In this section, results are presented for the analysis of transonic normal shock-wave/turbulent boundary-layer interactions in which the shock wave is of sufficient strength to separate the boundary layer. The detailed experimental data of Kooi[13,14] has been extensively used in this investigation to evaluate the present IBLT calculations with and without the inclusion of normal pressure gradients. Kooi performed a detailed experimental investigation of transonic shock-wave/boundary-layer interaction in the channel shown schematically in Fig. 3. A normal shock wave was established in this passage by placing a "choking wedge" on the lower flat plate; the choking wedge was positioned in the stream direction such that a normal shock wave emanated from the leading edge of the upper flat plate and impinged on the lower flat-plate boundary layer, which was tripped to turbulent near the leading edge as shown in Fig. 3. For $M_\infty = 1.4$, which is the case computed in the present investigation, Kooi experimentally deduced that the boundary-layer thickness δ_0^* on the lower surface, just upstream of interaction region, is 6.6 mm. This value of δ_0^* has been used to nondimensionalize all lengths in the present results and in the presentation of the experimental measurements of Kooi. The x coordinate has been redefined as $\bar{x} = (x - x_0^*)/\delta_0^*$ where x_0^* is the x location of the start of the interaction. A value of $x_0^* = 426$ mm has been inferred from Kooi's measurements[13] and has been used to scale the theoretical and experimental results.

For all calculations, the inviscid mesh consisted of 81 evenly distributed $\bar{x}$ grid points in the region $-4 \le \bar{x} \le 20$ and 21 y grid points nonuniformly distributed such that the smallest step size occurs at the wall. The outer inviscid boundary was placed at $y = 6.8$. Approximately eight points were placed in the boundary layer with the minimum $\Delta y = 0.0883$ located at the wall. The viscous calculation used the same streamwise mesh as the inviscid analysis to avoid the interpolation that was found in previous interaction

calculations[15] to cause oscillations. In the normal direction, 101 grid points were nonuniformly distributed from the wall across the viscous layer to $\hat{\eta} = 1.45$.

The IBLT calculations were performed in the computational region ABCD shown in Fig. 3, with the experimental pressure distribution imposed along the outer boundary to account for the boundary-layer blockage effect. In the present calculations, a converged solution was obtained first from a first-order IBLT analysis in which the pressure was assumed constant across the boundary layer. This calculation, in which $\bar{\omega} = 0.4$, required 50 global iterations to reduce the difference between the viscous and inviscid prediction for u_e to 10^{-3}. These results were then used to initialize the IBLT calculation with normal pressure gradients. In the latter calculation, it was found necessary to reduce $\bar{\omega}$ to 0.2 to obtain convergence, which was achieved in typically 20 additional global iterations. The reduction of the global relaxation factor is not surprising since the coupling between the viscous and inviscid flows is significantly greater with the inclusion of the numerical results for the equivalent inviscid flow in the viscous defect equations.

Figure 4 shows a comparison of the present computations from IBLT with the experimental data of Kooi[13] for the wall pressure, displacement thickness, and skin-friction coefficient for $M_\infty = 1.4$. Kooi used the same generalized definitions of the displacement thickness in presenting his experimental results as have been used in the present theoretical study. The skin-friction coefficient is based on the flow properties at the boundary-layer edge, which in the calculations has been defined where $F = 0.995F_i$ and in the experiment as the point where the pitot pressure became constant. The position of the imposed normal shock wave is indicated in Fig. 4.

The computed results, which were obtained with both the CS and modified CS turbulence models with the pressure varying (denoted by $p_y \neq 0$ in Fig. 4) across the boundary layer, will be discussed first. Figures 4a and 4b show that good agreement is obtained with the data with the present

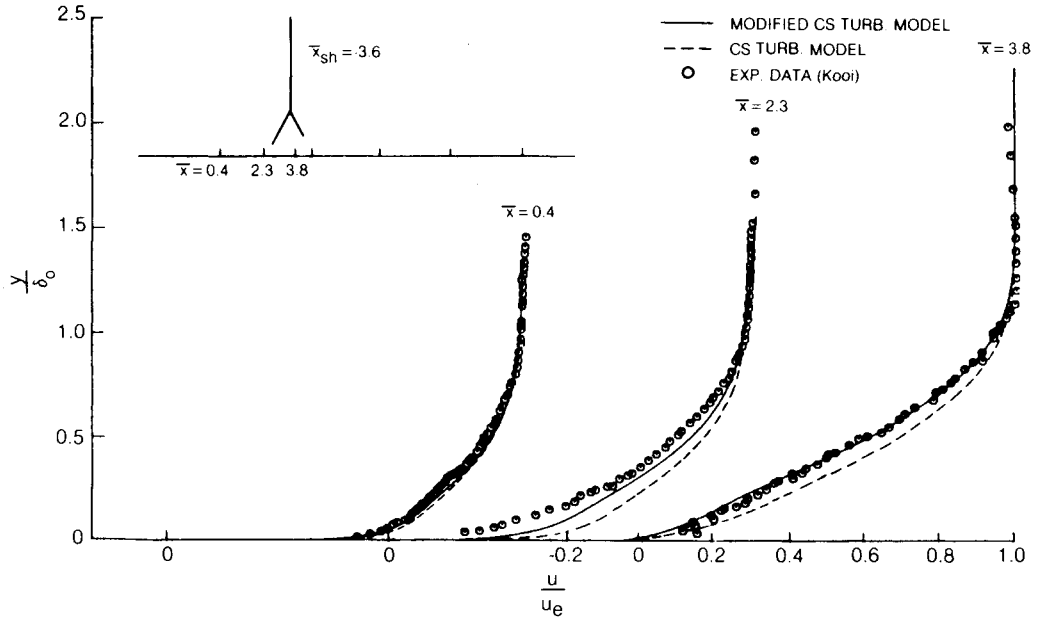

a) $x = 0.4$, 2.3, and 3.8.

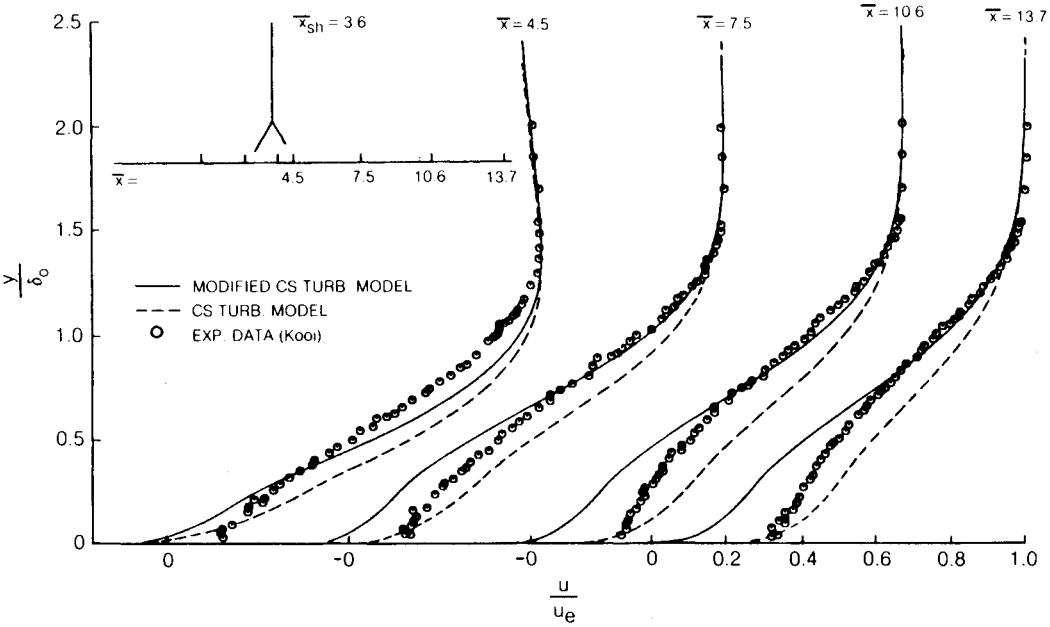

b) $x = 4.5$, 7.5, 10.6, and 13.7.

Fig. 5 Comparison of velocity profiles from IBLT ($p_y \neq 0$) with experimental data for $M_\infty = 1.4$ and $Re_\infty = 2.97 \times 10^5$.

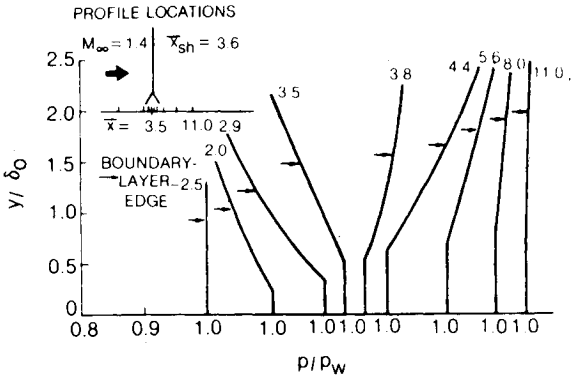

Fig. 6 Variation of pressure across boundary layer from equivalent inviscid flow (EIF) for transonic normal shock-wave/boundary-layer interaction.

IBLT using the modified CS turbulence model. Comparison of Figs. 4a and 4b shows that the turbulence model modification simultaneously improves the agreement for the wall pressure and the displacement thickness, which substantiates the use of the displacement body concept in separated flows. The comparison of the skin-friction results obtained with the CS and modified CS turbulence models shows good agreement with the data in the approach to the separation point occurring just upstream of the location of the imposed normal shock wave. However, downstream the modified model underpredicts the experimental skin friction and, therefore, predicts a larger separated flow region than that found experimentally. Modification to the outer region of the CS turbulence model has resulted in an improved prediction of the wall pressure and displacement thickness; the lack of agreement for the skin friction indicates that further work is required to correspondingly improve the accuracy of the IBLT with the modified CS turbulence model in the near wall region.

One of the advantages of the present approach is that IBLT computations can be made with and without normal pressure gradients in order to assess the relative importance of including pressure variations across the viscous layer. Figure 4 also shows the wall pressure, displacement thickness, and skin friction computed from IBLT without normal pressure gradients. This calculation was made with the modified CS turbulence model. Comparison of the results in Fig. 4 shows that the effect of including normal pressure gradients is relatively minor and has less of an impact on the results than the change in the turbulence model discussed previously. Although the present treatment of normal pressure gradients is an approximate one, it appears from these calculations that the dominant viscous effect in the prediction of separated transonic shock-wave/boundary-layer interaction is the inclusion of displacement thickness interaction. The solutions shown in Fig. 4 demonstrate that meaningful results can be obtained with IBLT without the inclusion of normal pressure gradients. The remaining results shown will be from the IBLT analysis that included normal pressure gradients.

Figure 5 shows a comparison of the computed and the experimental profiles for the u component of velocity at seven streamwise locations upstream and downstream of the normal shock wave. The insert in Fig. 5 shows the $\bar{x}$ location of these profiles; the corresponding station number used by Kooi[13] to label these profiles has also been included. Linear streamwise interpolation was used in the calculations to obtain the computed profiles at the same $\bar{x}$ location as those of the experimental measurements. The edge velocity u_e used to normalize the u profile was determined by the same criterion mentioned earlier for the respective theoretical and experimental boundary-layer thicknesses.

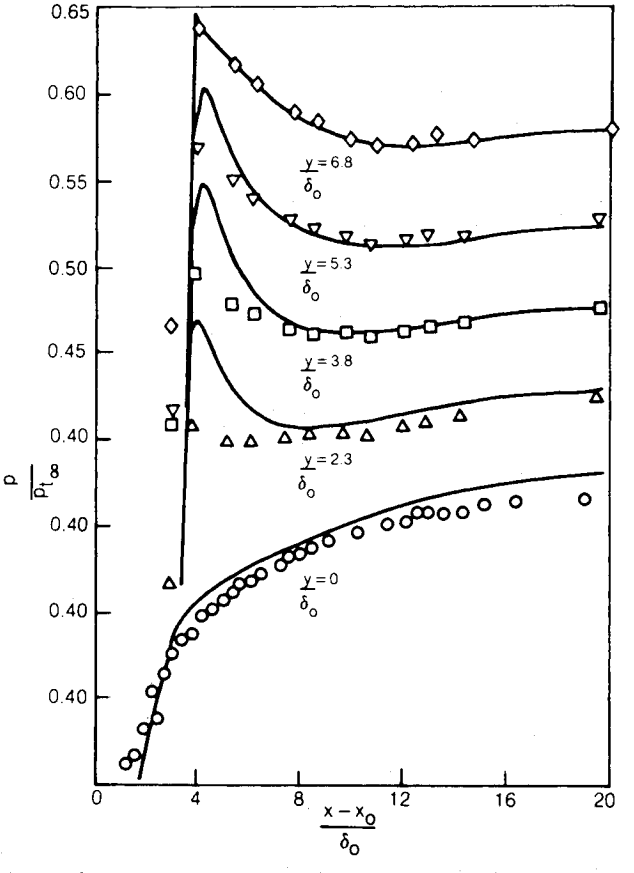

Fig. 7 Comparison of streamwise pressure distributions from IBLT ($p_y \neq 0$) and experimental data.

The velocity profiles shown in Fig. 5 illustrate the rapid changes that occur in turbulent boundary-layer profile due to an incident normal shock wave. For example, comparison of the experimental profile at $\bar{x} = 0.4$ with that just downstream of the shock wave at $\bar{x} = 3.8$ shows the enormous change that occurs in only three upstream boundary-layer thicknesses. The velocity profiles in Fig. 5 show that the IBLT results obtained with the modified CS turbulence model are in overall better agreement with the experimental data than those results obtained without this modification. The agreement is particularly good in the outer region of the turbulent boundary layer where this modification was made. Downstream of the shock wave the modified model underpredicts the velocity recovery in the near wall region as was expected from the skin-friction comparisons shown in Fig. 4. The results obtained with the unmodified model show a higher velocity in the wall region at each location than the modified model, which is consistent with the skin friction difference shown in Fig. 4. Despite the complexity of this flow, it is observed in Fig. 5 that the overall growth of the viscous layer, which appears to have a distinct edge, is well predicted by the present IBLT with the modified CS turbulence model.

The variation of the pressure across the boundary layer from the EIF is shown in Fig. 6 for selected streamwise stations both upstream and downstream of the shock wave, which is located at $\bar{x} = 3.6$. The $\bar{x}$ location of each of these normalized pressure profiles is shown in a scaled drawing inserted into Fig. 6. Since the variation in the static pressure across the viscous layer was insensitive to the turbulence model, only the IBLT results with the modified CS turbulence model are shown in Fig. 6. The arrows on each of the profiles are the edge of the viscous layer. The kink in the profiles near the wall is at the displacement thickness since, as was discussed earlier, the pressure was assumed constant from δ^* to the wall. Figure 6 shows the anticipated trend in

the static pressure variation in that, in the immediate vicinity of the shock wave, the pressure decreases with increasing y upstream of the shock wave and increases with increasing y downstream of the shock wave. The variation of the static pressure across the viscous layer reaches a maximum of about 10% in the immediate vicinity of the impinging shock wave; as expected, this variation vanishes upstream and downstream of this region as the flow returns to that of a conventional constant-pressure boundary layer.

Figure 7 shows a comparison of the computed and measured static pressure distributions at various y levels in the flowfield. The IBLT results shown are those obtained with the modified CS turbulence model. As mentioned previously, the static pressure distribution at $y=6.8$, which is the location of the outer inviscid computational boundary, was set equal to that measured by Kooi[13] in order to account for the effect of boundary-layer blockage. At the other y locations shown in Fig. 7, the agreement of the IBLT result with the experiment is good, except just downstream of the shock wave where the pressure rise is overpredicted. This overprediction in the interior of the flow may be due to the neglect of the entropy rise across the shock wave.

Conclusions

In this paper, a technique based on an interacting boundary-layer theory (IBLT) has been presented for the analysis of transonic shock-wave/boundary-layer interaction with particular emphasis on turbulent separated flow. In this technique, a finite difference solution of the viscous-layer equations, expressed in a defect form, is iteratively solved with the finite difference form of the inviscid stream function equation. Normal pressure gradients and imbedded shock effects have been included in the viscous-layer analysis by assuming that the pressure in this region is the same as that of the inviscid flow above the displacement thickness. In this paper, IBLT calculations for separated flow along with detailed comparisons with experimental data lead to the conclusions presented below.

The major conclusion drawn from the present work is that this displacement thickness interaction is the dominant effect which must be included in a viscous-inviscid interaction scheme for the prediction of transonic shock-wave/boundary-layer interaction where the shock is of sufficient strength to separate the turbulent boundary layer. Comparisons with the $M_\infty = 1.4$ case measured by Kooi indicate that, for this separated flow, the computed results show greater sensitivity to the turbulence model than to whether or not normal pressure gradients are included in the analysis. In this case, the pressure was found to vary by only about 10% across the viscous layer; hence, it is not surprising that the IBLT calculations proved to be relatively insensitive to whether or not this effect was included. In the future, additional data comparisons should be made, particularly as the shock strength is increased, to further substantiate this conclusion.

Favorable comparisons have been obtained with the present IBLT for Kooi's data for the pressure, displacement thickness, and velocity profiles in which a modified Cebeci-Smith turbulence model has been used. This modification, which is a straightforward change in the length scale in the outer region, provides encouragement that a simple eddy viscosity model may be adequate for the prediction of many of the flow properties in a turbulent separated flow. However, the skin-friction comparison indicates that further work is needed to improve this model in the inner or wall region.

Acknowledgments

The work reported in this paper was supported by the U.S. Air Force Office of Scientific Research under Contract F49620-81-C-0041. In addition, the authors acknowledge the interest and technical guidance provided by Dr. M. J. Werle of the United Technologies Research Center during the course of this work.

References

[1]Melnik, R. E. and Grossman, B., "Analysis of the Interaction of a Weak Normal Shock Wave with a Turbulent Boundary Layer," AIAA Paper 74-598, 1974.

[2]Adamson, T. C. Jr. and Feo, A., "Interaction Between a Shock Wave and a Turbulent Boundary Layer in Transonic Flow," *SIAM Journal of Applied Mathematics*, Vol. 29, 1975, pp. 121-145.

[3]Messiter, A. F., "Interaction Between a Normal Shock Wave and Turbulent Boundary Layer at High Transonic Speeds, Part I: Pressure Distribution," NASA CR-3194, 1979.

[4]Viegas, J. R. and Horstman, C. C., "Comparison of Multiequation Turbulence Models for Several Shock Boundary-Layer Interaction Flows," *AIAA Journal*, Vol. 17, Aug. 1979, pp. 811-820.

[5]Shea, J. R. III, "A Numerical Study of Transonic Normal Shock—Turbulent Boundary Layer Interactions," AIAA Paper 78-1170, 1978.

[6]Adamson, T. C. Jr. and Messiter, A. F., "Analysis of Two-Dimensional Interactions Between Shock Waves and Boundary Layers," *Annual Review of Fluid Mechanics*, 1980, pp. 103-138.

[7]LeBalleur, J. C., "Strong Matching Method for Computing Transonic Viscous Flows Including Wakes and Separations, Lifting Airfoils," *La Recherche Aerospatiale*, No. 1981-3 (English edition), 1981.

[8]East, L. F., "A Representation of Second-Order Boundary Layer Effects in the Momentum Integral Equation and in Viscous-Inviscid Interactions," Royal Aircraft Establishment, England, Tech. Rept. 81002, 1981.

[9]Lock, R. C. and Firmin, M. C. P., "Survey of Techniques for Estimating Viscous Effects in External Aerodynamics," Royal Aircraft Establishment, England, Tech. Memo. Aero 1900, April 1981.

[10]Carter, J. E., Edwards, D. E., and Hafez, M. M., "Analysis of Transonic Shock Induced Separated Flow Including Normal Pressure Gradients," AFOSR Rept. TR-83-1283, Oct. 1983.

[11]Carter, J. E., "A New Boundary-Layer Inviscid Iteration Technique for Separated Flow," AIAA Paper 79-1450, July 1979.

[12]Hafez, M. M. and Lovell, D., "Numerical Solution of the Transonic Stream Function Equation," *AIAA Journal*, Vol. 21, March 1983, pp. 327-335.

[13]Kooi, J. W., "Experiment on Transonic Shock-Wave Boundary Layer Interaction." AGARD CP-168, 1975.

[14]Kooi, J. W., "Influence of Free-Stream Mach Number on Transonic Shock Wave Boundary Layer Interaction," National Aerospace Laboratory, the Netherlands, Rept. NLR MP 78013 U, 1978.

[15]Carter, J. E. and Vatsa, V. N., "Analysis of Separated Boundary Layer Flows," Paper presented at the Eighth International Conference on Numerical Methods in Fluid Dynamics, Aachen, FRG, June 1982.

[16]Cebeci, T. and Smith, A. M. O., *Analysis of Turbulent Boundary Layers*, Academic Press, New York, 1974.

[17]Shang, J. S. and Hankey, W. L. Jr., "Numerical Solution for Supersonic Turbulent Flow Over a Compression Ramp," *AIAA Journal*, Vol. 13, 1975, pp. 1368-1374.

[18]Carter, J. E., "Viscous-Inviscid Interaction Analysis of Transonic Turbulent Separated Flow," AIAA Paper 81-1241, June 1981.

[19]Clauser, F. H., "The Turbulent Boundary Layer," *Advances in Applied Mechanics*, Vol. 4, 1956, pp. 1-51.

[20]Edwards, D. E., "Analytical Study of Turbulent Separated Flow," United Technologies Research Center, East Hartford, CT, to be published.

[21]Simpson, R. L., Chew, T. T., and Shivaparsad, B. G., "The Structure of a Separating Turbulent Boundary Layer, Part 1, Mean Flow and Reynolds Stresses," *Journal of Fluid Mechanics*, Vol. 113, 1981, pp. 23-51.